



Working Paper

## hp FEM for incompressible fluid flow - stable and stabilized

**Author(s):**

Gerdes, K.; Schötzau, Dominik

**Publication Date:**

1997

**Permanent Link:**

<https://doi.org/10.3929/ethz-a-004284950> →

**Rights / License:**

[In Copyright - Non-Commercial Use Permitted](#) →

This page was generated automatically upon download from the [ETH Zurich Research Collection](#). For more information please consult the [Terms of use](#).

# *hp* FEM for Incompressible Fluid Flow — Stable and Stabilized

K. Gerdes\*      D. Schötzau†

Seminar für Angewandte Mathematik, ETH Zürich  
CH-8092 Zürich, Switzerland

April 1998

Research Report No. 97-18

## Abstract

The stable Galerkin formulation and a stabilized Galerkin Least Squares formulation for the Stokes problem are analyzed in the context of the *hp*-version of the Finite Element Method (FEM). Theoretical results for both formulations establish exponential rates of convergence under realistic assumptions on the input data. We confirm these results by intensive numerical studies on an *L*-shaped domain where the solution exhibits corner singularities.

**Key words:** *hp* Finite Element Method (*hp*-FEM), Stokes problem, Galerkin formulation, Galerkin Least Squares formulation

AMS Subject Classifications

Primary: 65N30, 65N35

Secondary: 65N50

---

\*e-mail: gerdes@sam.math.ethz.ch

†e-mail: schoetz@sam.math.ethz.ch

# 1 Introduction

The efficient numerical solution of problems in fluid mechanics is of significant engineering interest. There are basically two reasons why the Finite Element approximation of such problems turns out to be difficult: Firstly, the presence of corner singularities and boundary layers in the solutions requires properly designed meshes. Secondly, the design of stable methods is a non-trivial issue. Intrinsic stability problems arise in the variational formulations due to incompressibility constraints or due to strongly convective terms.

Let us first discuss briefly the question of approximability: Although the solutions of fluid flow problems exhibit boundary layer or corner singularity phenomena, they are typically piecewise analytic. In that case it is well known, see e.g. [5, 20, 35, 37] and the references therein, that exponential rates of convergence can be obtained by the use of the  $hp$  version of a stable Finite Element Method (FEM). That is, in the case of corner singularities, by the use of an increasing polynomial approximation order and of meshes that are refined geometrically towards the singularities. One of the first implementations of  $hp$  methods for problems in fluid mechanics was developed by Oden et al. [23] during the 80ies. Their implementation has also been the basis of the commercial code PHLEX of COMCO Corp. in Austin, TX. The original code has recently been developed into the general and object oriented code HP90 [14] which we use for our numerical experiments.

In this work, stability aspects in the numerical approximation of Stokes flow are addressed in the context of  $hp$  FEM. In particular, we compare *stable* and *stabilized* schemes. The Stokes equations describe viscous incompressible fluid flow at moderate Reynolds number (or, alternatively, isotropic incompressible materials). These equations have become a very important model problem in computational fluid dynamics, as discretizations for Stokes flow based on mixed *Galerkin* formulations have to face some of the stability problems that are also encountered when solving the full incompressible Navier-Stokes equations (NSE). Namely, in order to fulfill the incompressibility constraint at the discrete level the velocity and pressure spaces cannot be chosen independently. Stability is only guaranteed as long as the discrete Babuška-Brezzi or inf-sup condition is satisfied by the velocity and the pressure spaces. This condition has been established for various velocity and pressure pairings (see, e.g., [12, 19, 24, 38] and the references there for the  $h$ -version FEM; and [8, 9, 34, 36, 39] and the references there for the  $p$ -,  $hp$ -version and spectral FEM). The use of  $hp$  methods for classical mixed Galerkin formulations with *stable* velocity and pressure space pairs (of different approximation order) is already well established in the FE community. Sophisticated  $hp$  and spectral element codes have been developed and many issues of practical importance have been addressed. We mention here only [13, 22, 26, 27, 28, 29, 30, 32, 42] and the references therein. In particular, adaptivity and a-posteriori error estimation aspects are dealt with in [1, 26, 28, 42], and domain decomposition and parallelization aspects are analyzed in [29, 30]. For  $hp$ /spectral implementations based on unstructured triangular meshes we refer to [22, 32] and the references therein.

Unfortunately, implementationally very attractive pairings, such as equal-order elements for the velocity and the pressure, do not fulfill the Babuška-Brezzi stability condition and lead to unphysical spurious pressure modes in computations. This inspired the development of numerous methods where the inf-sup condition is relaxed. We mention

here [27, 42], where penalty methods combined with reduced integration are analyzed in the  $hp$  context and exponential convergence is numerically observed. In [28, 42] a three-step  $hp$  adaptive strategy is proposed (based on pressure projection-correction methods) where equal-order elements can be used. Splitting schemes are also known in the spectral context (see, e.g., [13, 32] and the references therein).

In the pioneering work [21] a *stabilized* approach based on a *Galerkin Least Squares* formulation (GLS) has been presented by Hughes and his coworkers. The idea is to augment the bilinear form stemming from a Galerkin approach with appropriately weighted residuals of the differential equation. This method features in particular the possibility of equal-order interpolation for velocity and pressure. Closely related GLS-methodologies have already been applied successfully to a variety of problems in fluid flow, elasticity and continuum mechanics (see, e.g., [11, 15, 17, 21] and the references there). We also refer to the survey article [16].

However, the above mentioned GLS-stabilized methods have all been formulated in the context of the  $h$ -version of the FEM, i.e. the convergence is obtained by reducing the meshsize  $h$  at a fixed (low) polynomial degree which results in algebraic rates of convergence. Only most recently there have been attempts to extend the idea of GLS-stabilized methods to the context of the  $hp$  or spectral FEM. In [18] stabilized spectral element methods have been applied to solve the linearized NSE. However, no exponential rates of convergence have been proved and the analysis is confined to quasiuniform meshes. In [33] the authors presented a stabilized method of GLS type and exponential rates of convergence for equal-order interpolation in the velocities and pressure are established for singular solutions (see also Theorem 2.4 ahead). The same method has been analyzed in [10] where the error analysis gives algebraic rates of convergence for the  $p$  FEM but is restricted by regularity assumptions that are unrealistic in many practical situations.

In this paper we present the  $hp$  version of a stabilized method of Galerkin Least Squares type for the Stokes problem. The comparison of this  $hp$ -GLS Finite Element Method with the classical mixed Galerkin formulation is the goal of this paper. Both formulations lead to exponential rates of convergence under realistic assumptions on the input data and the mesh design. We present the theoretical results and confirm the exponential convergence of the  $hp$  FEM by an intensive numerical convergence study. We emphasize in this context the practical (implementational) advantages and disadvantages of both methods.

The outline of the paper is as follows: In Section 2 we establish the precise weak formulations and the  $hp$  FE spaces. With this setting we state the exponential convergence results for the Galerkin and GLS  $hp$ -FEM. In Section 3 we reveal details of the stabilized and the mixed  $hp$ -FE implementation. In Section 4 we define model problems that we use in our numerical convergence studies and present our numerical results. We finish the presentation with a comparison of the Galerkin and GLS  $hp$  FEM together with conclusions in Section 5.

## 2 Stable and stabilized $hp$ FEM for Stokes flow

In this section we briefly present the mathematical background concerning the  $hp$  Finite Element discretization of Stokes flow. First we review the Stokes equations and their

mixed formulation. Then we introduce  $hp$ -FE spaces and discretize the Stokes problem using first a Galerkin approach satisfying the Babuška-Brezzi stability condition and then a Galerkin Least Squares approach. We finally show that both schemes may lead to exponential rates of convergence.

## 2.1 The Stokes problem

In a bounded polygonal domain  $\Omega \subset \mathbb{R}^2$  we consider the Stokes boundary value problem for viscous incompressible fluid flow: Find a velocity field  $\vec{u}$  and a pressure  $p$  such that

$$-\nu \Delta \vec{u} + \nabla p = \vec{f} \quad \text{in } \Omega, \quad (2.1)$$

$$\nabla \cdot \vec{u} = 0 \quad \text{in } \Omega, \quad (2.2)$$

$$\vec{u} = \vec{0} \quad \text{on } \partial\Omega. \quad (2.3)$$

Here,  $\nu > 0$  is the kinematic viscosity which is related to the Reynolds number  $\text{Re}$  of the flow by  $\nu = 1/\text{Re}$ . The right hand side  $\vec{f}$  is a given body force per unit mass. We restrict ourselves in (2.3) to homogeneous boundary conditions, inhomogeneous ones are treated in the usual way (see, e.g., [40]).

On  $\Omega$  we use the space  $L^2(\Omega)$  of real-valued square-integrable functions, and we introduce its subspace

$$L_0^2(\Omega) = \{f \in L^2(\Omega) : \int_{\Omega} f(x) dx = 0\}$$

of functions with vanishing mean value. We denote by  $H^1(\Omega)$  the standard Sobolev space of order 1, and by  $H_0^1(\Omega)$  its subspace of all functions vanishing on the boundary  $\partial\Omega$  (in the sense of trace). Both spaces are provided with the usual norms and seminorms, and  $(\cdot, \cdot)$  is the  $L^2(\Omega)$  inner product.

The weak mixed formulation of (2.1)-(2.3) is to find a velocity field  $\vec{u} \in H_0^1(\Omega)^2$  and a pressure  $p \in L_0^2(\Omega)$  such that

$$\nu(\nabla \vec{u}, \nabla \vec{v}) - (\nabla \cdot \vec{v}, p) = (\vec{f}, \vec{v}), \quad (2.4)$$

$$(\nabla \cdot \vec{u}, q) = 0 \quad (2.5)$$

for all  $(\vec{v}, q) \in H_0^1(\Omega)^2 \times L_0^2(\Omega)$ . The equations (2.4)-(2.5) are equivalent to the problem: Find  $(\vec{u}, p) \in H_0^1(\Omega)^2 \times L_0^2(\Omega)$  such that

$$B_0(\vec{u}, p; \vec{v}, q) = F_0(\vec{v}, q) \quad \text{for all } (\vec{v}, q) \in H_0^1(\Omega)^2 \times L_0^2(\Omega), \quad (2.6)$$

where the bilinear form  $B_0$  and the functional  $F_0$  (defined on  $H^1(\Omega)^2 \times L^2(\Omega)$ ) are given by

$$B_0(\vec{u}, p; \vec{v}, q) = \nu(\nabla \vec{u}, \nabla \vec{v}) - (\nabla \cdot \vec{v}, p) - (\nabla \cdot \vec{u}, q), \quad (2.7)$$

$$F_0(\vec{v}, q) = (\vec{f}, \vec{v}). \quad (2.8)$$

It is well known (see, e.g., [12, 19]) that for  $\vec{f} \in L^2(\Omega)^2$  there exists a unique weak solution  $(\vec{u}, p)$  of (2.6) due to the (continuous) inf-sup condition

$$\inf_{0 \neq q \in L_0^2(\Omega)} \sup_{0 \neq \vec{v} \in H_0^1(\Omega)^2} \frac{(\nabla \cdot \vec{v}, q)}{\|\vec{v}\|_{H^1(\Omega)} \|q\|_{L^2(\Omega)}} \geq C = C(\Omega) > 0. \quad (2.9)$$

## 2.2 The $hp$ FE spaces

A mesh  $\mathcal{T}$  on the polygon  $\Omega \subset \mathbb{R}^2$  is a partition of  $\Omega$  into disjoint and open quadrilateral and/or triangular elements  $\{K\}$  such that  $\bar{\Omega} = \cup_{K \in \mathcal{T}} \bar{K}$ . The mesh  $\mathcal{T}$  is called regular if the intersection  $\bar{K} \cap \bar{K}'$  of two elements  $K$  and  $K'$  is either empty, a single vertex or an entire side. Otherwise, the mesh is irregular and contains hanging nodes and we restrict ourselves to 1-irregular meshes only. We denote, as usual, by  $h_K$  the diameter of  $K$  and by  $\rho_K$  the diameter of the largest circle inscribed into  $K$ . The fraction  $\sigma_K = h_K/\rho_K$  is called the aspect ratio of  $K$ . We consider only  $\kappa$ -uniform mesh families where there exists a constant  $\kappa > 0$  such that

$$\max_{K \in \mathcal{T}} \sigma_K \leq \kappa < \infty.$$

The meshwidth  $h$  of  $\mathcal{T}$  is  $h(\mathcal{T}) = \max_{K \in \mathcal{T}} \{h_K\}$ .  $\mathcal{T}$  is quasi-uniform if there exists  $\kappa_1, \kappa_2 > 0$  such that

$$\kappa_1 h(\mathcal{T}) \leq h_K \leq \kappa_2 \rho_K \quad \forall K \in \mathcal{T}.$$

We assume that for each  $K \in \mathcal{T}$  there is a diffeomorphism  $F_K$  such that  $K = F_K(\hat{K})$  where  $\hat{K}$  is a generic reference element which is either the reference triangle  $\hat{T} = \{(x, y) : 0 < x < 1, 0 < y < x\}$  or the reference square  $\hat{Q} = (0, 1)^2$ . The mesh  $\mathcal{T}$  is called affine if it only consists of triangles and parallelograms. In that case the mappings  $F_K$  are affine transformations. Let now

$$\underline{k} = \{k_K : K \in \mathcal{T}\} \tag{2.10}$$

be a polynomial degree distribution on  $\mathcal{T}$  which associates with each element  $K \in \mathcal{T}$  an elemental polynomial degree  $k_K$ . We then introduce the  $hp$ -FE spaces

$$S^{\underline{k},0}(\mathcal{T}) = \{f \in L^2(\Omega) : f|_K \circ F_K \in \mathcal{S}^{k_K}(\hat{K}), K \in \mathcal{T}\}, \tag{2.11}$$

$$S^{\underline{k},1}(\mathcal{T}) = \{f \in H^1(\Omega) : f|_K \circ F_K \in \mathcal{S}^{k_K}(\hat{K}), K \in \mathcal{T}\}. \tag{2.12}$$

Here,  $\mathcal{S}^k(\hat{K})$  denotes a generic polynomial space on  $\hat{K}$  which is to be understood as

$$S^k(\hat{K}) = \begin{cases} \mathcal{Q}^k(\hat{K}) & \text{if } \hat{K} \text{ is the reference square } \hat{Q} \\ \mathcal{P}^k(\hat{T}) & \text{if } \hat{K} \text{ is the reference triangle } \hat{T}, \end{cases} \tag{2.13}$$

where, on a domain  $D \subset \mathbb{R}^2$ ,  $\mathcal{P}^k(D)$  is the space of all polynomials of total degree  $\leq k$  and  $\mathcal{Q}^k(D)$  the set of all polynomials of degree  $\leq k$  in each variable.

The second index  $l$  for the spaces  $S^{\underline{k},l}(\mathcal{T})$  in (2.11)-(2.12) refers to the degree of continuity. The functions in  $S^{\underline{k},0}(\mathcal{T})$  are elementwise (mapped) polynomials that may be discontinuous across element boundaries. Functions in  $S^{\underline{k},1}(\mathcal{T})$  are piecewise (mapped) polynomials that are globally continuous. Implementationally, some care is required to ensure the interelement continuity in the space  $S^{\underline{k},1}(\mathcal{T})$  if  $k_K$  is variable. In some elements the external (or side) modes in the polynomial spaces must be reduced whereas the internal (or bubble) modes are of full degree  $k_K$ . This can be achieved by splitting  $k_K$  into edge- and bubble-degrees (cf. Section 3). If the polynomial degree is constant throughout the mesh  $\mathcal{T}$  (i.e.  $k_K = k \forall K \in \mathcal{T}$ ), we use the shorthand notations  $S^{k,1}(\mathcal{T})$  and  $S^{k,0}(\mathcal{T})$ . For a given polynomial degree vector  $\underline{k}$  we set  $|\underline{k}| = \max\{k_K : K \in \mathcal{T}\}$ .

## 2.3 Galerkin and Galerkin Least Squares discretizations

Let now  $\mathcal{T}$  be a (possibly irregular)  $\kappa$ -uniform and affine mesh on  $\Omega$  and let  $\underline{k} = \{k_K\} = \{k_K^v\}$  and  $\underline{k}^p = \{k_K^p\}$  be two polynomial degree distributions as in (2.10) for the velocity and the pressure, respectively. The FE-spaces  $\vec{V}_N$  and  $M_N$  that approximate the velocity and the pressure are then

$$\vec{V}_N = S^{k,1}(\mathcal{T})^2, \quad (2.14)$$

$$M_N = S^{k^p,l}(\mathcal{T}), \quad l = 0 \text{ or } l = 1. \quad (2.15)$$

Thus, for  $l = 0$  we admit discontinuous pressures whereas in the case  $l = 1$  we use continuous pressure interpolation. We define further

$$\vec{V}_{N,0} = \vec{V}_N \cap H_0^1(\Omega)^2, \quad M_{N,0} = M_N \cap L_0^2(\Omega). \quad (2.16)$$

The *Galerkin* discretization (G) of (2.6) is now:

Find a discrete velocity  $\vec{u}_N \in \vec{V}_{N,0}$  and a discrete pressure  $p_N \in M_{N,0}$  such that

$$B_0(\vec{u}, p; \vec{v}, q) = F_0(\vec{v}, q) \quad \text{for all } (\vec{v}, q) \in \vec{V}_{N,0} \times M_{N,0}, \quad (2.17)$$

where  $B_0$  and  $F_0$  are given in (2.7) and (2.8).

If the FE-spaces  $\vec{V}_N$  and  $M_N$  satisfy the following discrete inf-sup stability condition due to I. Babuška and F. Brezzi

$$\inf_{0 \neq q \in M_{N,0}} \sup_{\vec{v} \in \vec{V}_{N,0}} \frac{(\nabla \cdot \vec{v}, q)}{\|\vec{v}\|_{H^1(\Omega)} \|q\|_{L^2(\Omega)}} \geq \gamma(N) > 0, \quad (2.18)$$

then the problem (2.17) has a unique solution  $(\vec{u}_N, p_N) \in \vec{V}_{N,0} \times M_{N,0}$  and we have the error estimates

$$\|\vec{u} - \vec{u}_N\|_{H^1(\Omega)} \leq C\gamma(N)^{-1} \inf_{\vec{v} \in \vec{V}_{N,0}} \|\vec{u} - \vec{v}\|_{H^1(\Omega)} + C\nu^{-1} \inf_{q \in M_{N,0}} \|p - q\|_{L^2(\Omega)} \quad (2.19)$$

$$\|p - p_N\|_{L^2(\Omega)} \leq C\nu\gamma(N)^{-2} \inf_{\vec{v} \in \vec{V}_{N,0}} \|\vec{u} - \vec{v}\|_{H^1(\Omega)} + C\gamma(N)^{-1} \inf_{q \in M_{N,0}} \|p - q\|_{L^2(\Omega)} \quad (2.20)$$

with  $C = C(\Omega)$  independent of  $N$  and  $\nu$ . The inf-sup constant  $\gamma(N)$  enters in these estimates, and in order to obtain optimal error estimates in both the velocity and the pressure one should try to select the spaces  $\vec{V}_N$  and  $M_N$  in such a way that  $\gamma(N)$  depends as little as possible on the discretization parameter  $N$  (i.e. the meshwidths and the polynomial degrees). A possible choice are the “ $\mathcal{S}^k \times \mathcal{S}^{k-2}$ ” elements, that is

$$\vec{V}_N = S^{k,1}(\mathcal{T})^2, \quad M_N = S^{k-2,l}(\mathcal{T}) \quad (l = 0, 1), \quad (2.21)$$

where the difference between the velocity and pressure polynomial degree is always 2,  $k_K^p = k_K^v - 2 = k_K - 2$ . It is shown in [34, 35, 39] for regular and certain irregular meshes  $\mathcal{T}$  that these spaces satisfy the discrete inf-sup condition (2.18) with  $\gamma(N) \geq C |\underline{k}|^{-\beta}$  ( $C$  just depends on  $\Omega$  and the shape regularity constant  $\kappa$ ) where  $\beta = \frac{1}{2}$  if  $\mathcal{T}$  consists only of parallelograms, and with  $\beta = 3$  otherwise. These spaces do not lead to optimal error estimates in the  $h$ - or  $p$ -version of the FEM. However, exponential convergence in the  $hp$ -FEM can be achieved using “ $\mathcal{S}^k \times \mathcal{S}^{k-2}$ ” elements. Various other velocity and pressure

$hp$ -space pairs are known which are stable in the sense of (2.18) with  $\gamma(N)$  independent of the diameter of the elements but depending (algebraically) on the polynomial or spectral order (see, e.g., [39]). Most recently, Bernardi and Maday [9] proved that “ $\mathcal{Q}^k \times \mathcal{P}^{k-1}$ ” elements are even stable independently of the polynomial order  $k$  (on meshes consisting of parallelograms) and hence this choice leads to optimal error estimates in the  $h$ - or  $p$ -version FEM. Nevertheless, this choice seems to be not very attractive due to the additional complications in the implementation because quadrilateral and triangular degrees of freedom have to be used together on a quadrilateral mesh.

The easiest choice of the FE-spaces from an implementational point of view would be elements of equal polynomial order in the velocity and the pressure, i.e.

$$\vec{V}_N = S^{k,1}(\mathcal{T})^2, \quad M_N = S^{k,l}(\mathcal{T}) \quad (l = 0, 1), \quad (2.22)$$

with an identical degree distribution  $\underline{k}$  for both the velocity and the pressure. However, in that case the inf-sup constant  $\gamma(N)$  in (2.18) is zero [9]. In computations the violation of the inf-sup condition often leads to unphysical pressure oscillations and during the last decade this problem has been studied thoroughly. In the pioneering work [21] a possible relaxation of the Babuška-Brezzi condition based on a Galerkin Least Squares (GLS) approach that accomodates equal-order interpolation in the velocities and the pressure has been proposed. In the meantime these GLS-stabilizations techniques have already been applied successfully to a variety of problems in fluid mechanics and elasticity. However, most of the methods have been formulated in the context of the  $h$  version. We refer to [11, 15, 17, 21], to the survey article [16] and to the references there. Only most recently some attention has been turned to the issue of extending the schemes to the  $hp$  or spectral context (see [18, 10, 33]).

We consider here an  $hp$  approach of Galerkin Least Square type proposed by [10, 17, 21]. We define for an user-specified parameter  $\alpha \geq 0$  and the equal-order spaces in (2.22) an augmented bilinear form  $B_\alpha$  and a functional  $F_\alpha$  by

$$\begin{aligned} B_\alpha(\vec{u}, p; \vec{v}, q) &= \nu(\nabla \vec{u}, \nabla \vec{v}) - (\nabla \cdot \vec{v}, p) - (\nabla \cdot \vec{u}, q) \\ &\quad - \alpha \sum_{K \in \mathcal{T}} \frac{h_K^2}{k_K^4} (-\nu \Delta \vec{u} + \nabla p, -\nu \Delta \vec{v} + \nabla q)_K, \end{aligned} \quad (2.23)$$

$$F_\alpha(\vec{v}, q) = (\vec{f}, \vec{v}) - \alpha \sum_{K \in \mathcal{T}} \frac{h_K^2}{k_K^4} (\vec{f}, -\nu \Delta \vec{v} + \nabla p)_K. \quad (2.24)$$

Above,  $(\cdot, \cdot)_K$  is the  $L^2(K)$  inner product on the element  $K$ . The bilinear form  $B_\alpha$  is obtained by a modification of the original Galerkin form  $B_0$  in (2.7). The elementwise Galerkin Least Squares terms  $(-\nu \Delta \vec{u} + \nabla p, -\nu \Delta \vec{v} + \nabla q)_K$  containing residuals of the Stokes equation (2.1) are weighted by  $\alpha \delta_K = \alpha h_K^2 / k_K^4$  and added to  $B_0$ .  $F_\alpha$  is obtained analogously. The crucial point in connection with higher order methods is the proper choice of the mesh-dependent weights  $\delta_K$  in dependence on the approximation order  $k_K$ . Note that for  $\alpha = 0$  the form  $B_\alpha$  equals  $B_0$ . The choice of  $\alpha$  is completely independent of the element sizes  $h_K$  and the polynomial degrees  $k_K$  (see also Section 4.2 ahead).

The *Galerkin Least Squares* (GLS) formulation is:

Find a discrete velocity  $\vec{u}_N \in \vec{V}_{N,0}$  and a pressure  $p_N \in M_{N,0}$  such that

$$B_\alpha(\vec{u}_N, p_N; v, q) = F_\alpha(\vec{v}, q) \quad \text{for all } (v, q) \in V_{N,0} \times M_{N,0}. \quad (2.25)$$

Again, for  $\alpha = 0$ , (2.25) reduces to the Galerkin approach given in (2.17). The GLS-method (2.25) was analyzed in the context of the  $h$ -version FEM in [17, 21] and optimal error estimates for the velocity and pressure were established. In [10] it is investigated in the  $hp$  context and the error analysis given there results in algebraic rates of convergence for the  $p$  FEM but is restricted by regularity assumptions that are unrealistic in many practical situations. In [33] the  $hp$ -version (2.25) is analyzed for singular solutions.

The stability of (2.25) is also addressed in [33]: Under the assumption that  $k_K \geq 2$  there exists a constant  $\alpha_{max}$  (not known in general and depending on  $\nu$  but independent of the element size  $h_K$  and the approximation orders  $k_K$ ) such that for  $0 < \alpha < \alpha_{max}$

$$\sup_{(\vec{0}, 0) \neq (\vec{v}, q) \in \vec{V}_{N,0} \times M_{N,0}} \frac{B_\alpha(\vec{u}, p; \vec{v}, q)}{(\|\vec{u}\|_{H^1(\Omega)}^2 + \|p\|_{L^2(\Omega)}^2)^{\frac{1}{2}} (\|\vec{v}\|_{H^1(\Omega)}^2 + \|q\|_{L^2(\Omega)}^2)^{\frac{1}{2}}} \geq C \frac{\alpha}{|\underline{k}|^4} \quad (2.26)$$

for all  $(\vec{0}, 0) \neq (\vec{u}, p) \in \vec{V}_{N,0} \times M_{N,0}$  with  $C$  independent of  $\alpha$ ,  $\underline{k}$ , and the meshwidths. As a consequence, (2.25) has an unique solution. Different polynomial degree distributions for the velocity and the pressure as in (2.14)-(2.15) are of course also imaginable in (2.22), but not that attractive from an impementational point of view.

## 2.4 Exponential convergence results

If the right hand side  $\vec{f}$  in (2.1) is analytical in the closure  $\overline{\Omega}$  of  $\Omega$  it follows that  $\vec{u}$  and  $p$  are analytical in  $\overline{\Omega} \setminus \cup_{i=1}^M A_i$  where  $\{A_i\}_{i=1}^M$  denote the vertices of  $\Omega$ . However, there are corner singularities arising at the vertices of  $\Omega$ . It is well known for closely related elasticity and potential problems that under the analyticity assumption on the data the solutions belong to countably normed spaces  $B_\beta^l(\Omega)$  [3]. For the Stokes problem the corresponding regularity assumption is

$$\vec{u} \in B_\beta^2(\Omega)^2, \quad p \in B_\beta^1(\Omega), \quad \text{for some } \beta \in (0, 1). \quad (2.27)$$

We refer to [3] for the exact definition of these spaces which model the singular behaviour at the vertices and the analytical one in the interior. We emphasize that in general  $B_\beta^2(\Omega)^2 \not\subset H^2(\Omega)^2$  and  $B_\beta^1(\Omega) \not\subset H^1(\Omega)$ . In polar coordinates  $(r, \varphi)$  near a vertex  $A_i$  solutions  $(\vec{u}, p) \in B_\beta^2(\Omega)^2 \times B_\beta^1(\Omega)$  are typically of the form

$$\vec{u}(r, \varphi) = r^\lambda \vec{\Phi}(r, \varphi) + \text{smoother}, \quad p(r, \varphi) = r^{\lambda-1} \Psi(r, \varphi) + \text{smoother}, \quad (2.28)$$

for some  $\lambda \in (0, 1)$  and with  $\Psi$  and  $\vec{\Phi}$  analytical in  $\overline{\Omega}$ .

In order to capture the singular behaviour of  $(\vec{u}, p)$  near corners we introduce meshes that are geometrically refined towards the vertices  $\{A_i\}$ .

**Definition 2.1** *On the reference square  $\hat{Q} = (0, 1)^2$ , the basic geometric mesh  $\Delta_{n,\sigma}$  with grading factor  $\sigma \in (0, 1)$  and  $n + 1$  layers is created recursively as follows: If  $n = 0$ ,  $\Delta_{n,\sigma} = \{\hat{Q}\}$ .  $\Delta_{n+1,\sigma}$  is generated by subdividing the element  $K \in \Delta_{n,\sigma}$  with  $0 \in \overline{K}$  into four smaller rectangles by dividing its sides in a  $\sigma : (1 - \sigma)$  ratio. Thereby, the hanging nodes can be removed or not as indicated in Figure 1.*

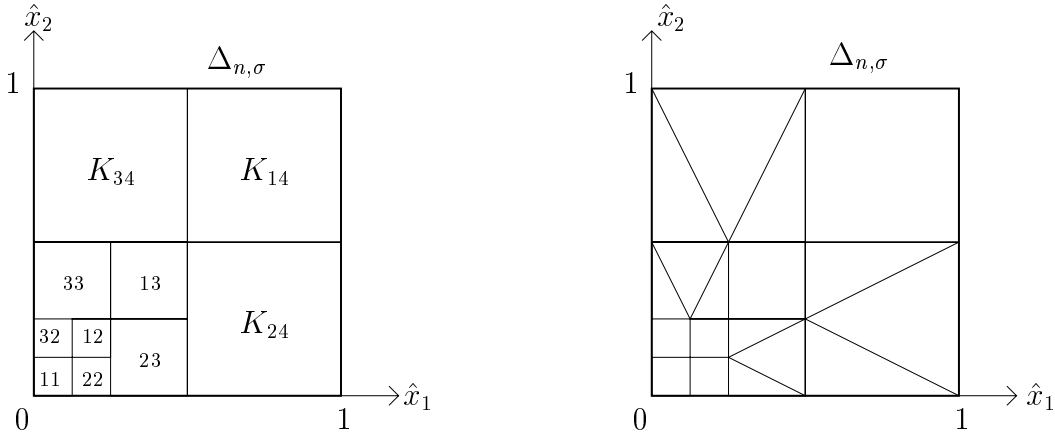


Figure 1: The basic geometric meshes  $\Delta_{n,\sigma}$  with  $n = 3$  and  $\sigma = 0.5$ .

Figure 1 depicts basic geometric meshes  $\Delta_{n,\sigma}$  on the reference square with  $n = 3$  and  $\sigma = 0.5$ . The quadrilateral elements in the left mesh are numbered as shown in Figure 1. The elements  $K_{1j}$ ,  $K_{2j}$  and  $K_{3j}$  constitute the layer  $j$ ,  $j = 2, \dots, n + 1$ . The layer 1 consists only of the smallest element  $K_{11}$  near the origin.

**Definition 2.2** *A geometric mesh  $\mathcal{T}_{n,\sigma}$  in the polygon  $\Omega \subseteq \mathbb{R}^2$  is obtained by mapping the basic geometric meshes  $\Delta_{n,\sigma}$  from  $\hat{Q}$  affinely to a vicinity of each convex corner of  $\Omega$ . At reentrant corners three suitably scaled copies of  $\Delta_{n,\sigma}$  are used (as is indicated in Figure 2). The remainder of  $\Omega$  is subdivided with a fixed affine quasi-uniform and regular partition.*

In Figure 2 this local geometric refinement is illustrated. For ease of exposition we consider only mesh patches that are identically refined with a fixed  $\sigma$  and  $n$ , although different grading factors and numbers of layers may be used for the partition of each corner patch. It is clear that also other geometric refinement strategies towards the vertices are imaginable.

We consider now polynomial degree distributions on geometric meshes which we also assume to be identical in each geometric corner patch.

**Definition 2.3** *A polynomial degree distribution  $\underline{k}$  on a geometric mesh  $\mathcal{T}_{n,\sigma}$  is called linear with slope  $\mu > 0$  if the elemental polynomial degrees are layerwise constant in the geometric patches and are given by  $k_j := \max(2, \lfloor \mu j \rfloor)$  in layer  $j$ ,  $j = 1, \dots, n + 1$ . In the interior of the domain the elemental polynomial degree is set constant to  $\max(2, \lfloor \mu(n + 1) \rfloor)$ .*

Under assumption (2.27) the following theorem establishes exponential rates of convergence.

**Theorem 2.4** *Let  $(\vec{u}, p)$  be the exact solution of the Stokes problem (2.1)-(2.3) satisfying (2.27). Let  $(\vec{u}_N, p_N)$  be the discrete solution of the G- or GLS-formulation obtained on a geometric mesh  $\mathcal{T}_{n,\sigma}$  with a linear degree vector. Then there exists a  $\mu_0 > 0$  such that*

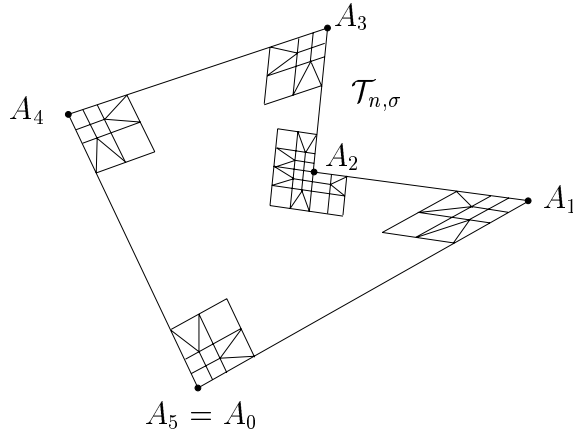


Figure 2: A geometric mesh  $\mathcal{T}_{n,\sigma}$  on  $\Omega$ .

for linear degree vectors  $\underline{k}$  with slope  $\mu \geq \mu_0$ ,  $k_j = \max(2, \lfloor \mu j \rfloor)$ ,  $j = 1, \dots, n+1$ , the discrete solution  $(\vec{u}_N, p_N) \in \vec{V}_{N,0} \times M_{N,0}$  with  $\vec{V}_N = S^{\underline{k},1}(\mathcal{T}_{n,\sigma})^2$  and

$$M_N = \begin{cases} S^{\underline{k}-2,l}(\mathcal{T}_{n,\sigma}) & \text{for the G-method, } l = 0, 1 \\ S^{\underline{k},l}(\mathcal{T}_{n,\sigma}) & \text{for the GLS-method with } 0 < \alpha < \alpha_{max}, l = 0, 1 \end{cases}$$

satisfies

$$\|\vec{u} - \vec{u}_N\|_{H^1(\Omega)} + \|p - p_N\|_{L^2(\Omega)} \leq C \exp(-bN^{\frac{1}{3}}). \quad (2.29)$$

Here,  $N = \dim(\vec{V}_N) \approx \dim(M_N)$  and the constants  $C$  and  $b$  are independent of  $N$ . In the case of the GLS-method the constant  $C$  depends on  $\alpha$ .

**Remark 2.5** In the Galerkin approach as well as in the GLS approach the pressure can be approximated continuously ( $l = 1$ ) or discontinuously ( $l = 0$ ). In both cases Theorem 2.4 holds true.

For the G-method and  $l = 0$  this result is proved in [36] using the  $hp$ -approximation results of [20]. The results in the case of the GLS-method for  $l = 0, 1$  can be found in [33]. The case  $l = 1$  for the G-scheme follows from a general approximation result in [33]. Note that the dependence on the viscosity  $\nu$  in (2.29) seems not to be known at present.

**Remark 2.6** If the polynomial degree is chosen to be constant throughout the mesh, i.e.  $k_K = k$  for all  $K \in \mathcal{T}$ , Theorem 2.4 still holds true: The exponential rates of convergence (2.29) are obtained by choosing  $k$  proportionally to the number of layers, that is  $k = \max(2, \lfloor \mu(n+1) \rfloor)$ .

## 2.5 $h$ -version and $p$ -version FEM

The weak formulations (2.17) and (2.25) are based on general  $hp$ -FE spaces such as the ones in (2.21) and (2.22). Exponential convergence in the  $hp$ -FEM is then obtained by

the use of geometric meshes and increasing polynomial degrees. But the  $h$ - and  $p$ -version of our two methods are also covered by the framework in Section 2.3. The spaces are chosen again as

$$\vec{V}_N = S^{k,1}(\mathcal{T})^2, \quad M_N = S^{k-2,l}(\mathcal{T}), \quad l = 0, 1$$

for the Galerkin approach and as

$$\vec{V}_N = S^{k,1}(\mathcal{T})^2, \quad M_N = S^{k,l}(\mathcal{T})^2, \quad l = 0, 1$$

for the Galerkin Least Squares scheme. (The index  $l$  indicates as before whether the pressure is approximated continuously or discontinuously.) The  $h$ -version is now obtained by fixing the (possibly low) polynomial degree  $k$  on a quasiuniform mesh  $\mathcal{T}$  of meshwidth  $h$ . The convergence is obtained by uniformly  $h$ -refining this mesh. The following optimal convergence rate for the  $h$ -version GLSFEM has been established in [17]

$$\|\vec{u} - \vec{u}_N\|_{H^1(\Omega)} + \|p - p_N\|_{L^2(\Omega)} \leq c \left( h^k |\vec{u}|_{H^{k+1}(\Omega)} + h^{k+1} |p|_{H^k(\Omega)} \right). \quad (2.30)$$

The corresponding convergence result for the  $h$ -version GFEM is [19, 36, 39]

$$\|\vec{u} - \vec{u}_N\|_{H^1(\Omega)} + \|p - p_N\|_{L^2(\Omega)} \leq c h^{k-1} \left( |\vec{u}|_{H^k(\Omega)} + |p|_{H^{k-1}(\Omega)} \right). \quad (2.31)$$

Here,  $|\cdot|_{H^l(\Omega)}$  denotes the usual semi-norm in the Sobolev space  $H^l(\Omega)$  of order  $l$ . However, the regularity assumptions in (2.30) and (2.31) are unrealistic in many practical situations due to corner singularities where only regularity assumptions as in (2.27) hold true.

Similarly, the  $p$ -version is obtained by fixing a quasiuniform grid  $\mathcal{T}$  and increasing continuously the polynomial degree  $k$ . We remark that the  $p$ -version convergence rates are suboptimal because the inf-sup constants in (2.18) and (2.26) depend on the polynomial degree (see [10] for GLSFEM and [36, 39] for GFEM). If the exact solution  $(\vec{u}, p)$  is analytical in the whole domain  $\bar{\Omega}$  (including the corners), the  $p$ -version leads also to exponential rates of convergence (which is not the case if the solution exhibits corner singularities as in (2.27)).

### 3 Implementational details

We concentrate from now on the following two discretizations of the Stokes problem which we implemented numerically and which we restate here shortly:

Let  $\underline{k}$  be a polynomial degree distribution on  $\mathcal{T}$ .

**The Galerkin formulation (G):** Let

$$\vec{V}_N = S^{\underline{k},1}(\mathcal{T})^2, \quad M_N = S^{\underline{k}-2,0}(\mathcal{T}).$$

The G-method is to find  $(\vec{u}_N, p_N) \in \vec{V}_{N,0} \times M_{N,0}$  such that

$$B_0(\vec{u}_N, p_N; \vec{v}, q) = F_0(\vec{v}, q) \quad \text{for all } (\vec{v}, q) \in \vec{V}_{N,0} \times M_{N,0}.$$

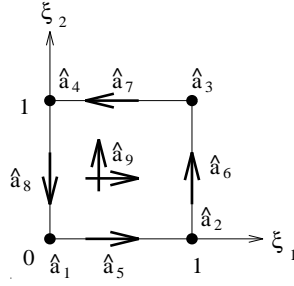


Figure 3: Quadrilateral reference element  $\hat{Q}$  with nodes  $(\hat{a}^1, \dots, \hat{a}^9)$ .

**The Galerkin Least Squares formulation (GLS):** Let

$$\vec{V}_N = S^{k,1}(\mathcal{T})^2, \quad M_N = S^{k,1}(\mathcal{T}).$$

The GLS-method is to find  $(\vec{u}_N, p_N) \in \vec{V}_{N,0} \times M_{N,0}$  such that

$$B_\alpha(\vec{u}_N, p_N; \vec{v}, q) = F_\alpha(\vec{v}, q) \quad \text{for all } (\vec{v}, q) \in \vec{V}_{N,0} \times M_{N,0}.$$

Observe that we consider a continuous pressure approximation in the GLSFEM while the pressure is discontinuously interpolated in the GFEM. This choice has been made since it points out the principal advantages of implementing GLSFEM: In the GLSFEM velocity and pressure are treated in exactly the same way. For the GFEM difficulties arise if one enforces different polynomial degrees for the velocity and the pressure and different interelement continuity requirements for  $\vec{u}_N$  and  $p_N$ .

Our  $hp$ -FE implementation for the Stokes problem is based on HP90, a flexible FE code for general elliptic problems in Fortran 90 [14]. HP90 allows for isotropic and anisotropic mesh refinements, both  $h$ - and  $p$ -refinements. In particular,  $h$ -refinements can lead to irregular meshes with hanging nodes and HP90 is designed to handle such meshes and enforces the appropriate continuity requirements by constraining these irregular nodes. We refer to [14, 23] for a detailed description of the constraining procedure.

In our numerical examples we use quadrilateral finite elements to discretize the domain  $\Omega$ . Implementationally, the elemental polynomial degrees  $k_K$  in (2.10) are further split into edge and internal degrees that can vary within the element, i.e.  $k_K$  is to be understood as the vector  $k_K = \{k_K^1, k_K^2, k_K^3, k_K^4, k_K^5\}$ . Here  $k_K^i$ ,  $i = 1, \dots, 4$ , is the polynomial degree on the  $i$ -th edge, and  $k_K^5$  the polynomial degree in the interior of the element. The nodes  $\hat{a}_K^1, \dots, \hat{a}_K^9$  correspond to  $k_K$ , where  $\hat{a}_K^1, \dots, \hat{a}_K^4$  denote the vertex nodes,  $\hat{a}_K^5, \dots, \hat{a}_K^8$  the mid-side nodes and  $\hat{a}_K^9$  is the middle node. This is shown schematically in Figure 3 for the reference square  $\hat{Q} = (0, 1)^2$ . The shape functions that are associated with the nodes  $\hat{a}_K$  of the reference element are the nodal based Lagrange shape functions but other shape functions can be used as well (cf. [14]).

In the case of the GLS method we need to interpret the reference element  $\hat{Q}$  as a vector valued reference element, i.e. we use the shape functions and degrees of freedom (dof) that correspond to  $\hat{Q}$  to approximate each velocity component and the pressure. The stabilization term in (2.23) involves second derivatives and therefore we also need the second derivatives of the reference element shape functions  $\varphi(\xi_1, \xi_2)$  with respect to the physical coordinates  $(x_1, x_2) = F_K(\xi_1, \xi_2)$ . In the case of an affine element mapping  $F_K$

the chain rule gives

$$\frac{\partial^2 \varphi}{\partial x_i^2} = \frac{\partial^2 \varphi}{\partial \xi_1^2} \left( \frac{\partial \xi_1}{\partial x_i} \right)^2 + \frac{\partial^2 \varphi}{\partial \xi_2^2} \left( \frac{\partial \xi_2}{\partial x_i} \right)^2. \quad (3.1)$$

But the terms  $\partial \xi_j / \partial x_i$  are not constant in the case of a general (e.g. bilinear) element mapping which leads to

$$\frac{\partial^2 \varphi}{\partial x_i^2} = \frac{\partial^2 \varphi}{\partial \xi_1^2} \frac{\partial \xi_1}{\partial x_i} + \frac{\partial \varphi}{\partial \xi_1} \frac{\partial^2 \xi_1}{\partial x_i^2} + \frac{\partial^2 \varphi}{\partial \xi_2^2} \frac{\partial \xi_2}{\partial x_i} + \frac{\partial \varphi}{\partial \xi_2} \frac{\partial^2 \xi_2}{\partial x_i^2}. \quad (3.2)$$

The terms  $\partial \xi_j / \partial x_i$  and  $\partial^2 \xi_j / \partial x_i^2$  are rational functions and can thus not be integrated exactly, but the use of a higher order integration rule reduces the error in the element computations. Nevertheless, the element computations are completely standard and for an element  $K$  the local element stiffness matrix  $E_{K,\alpha}$  and load vector  $F_{K,\alpha}$  result in an element system of equations that is of the well known form

$$E_{K,\alpha} \begin{bmatrix} \vec{u} \\ p \end{bmatrix} = \begin{bmatrix} A_\alpha & 0 & B_{1,\alpha}^t \\ 0 & A_\alpha & B_{2,\alpha}^t \\ B_{1,\alpha} & B_{1,\alpha} & \alpha M \end{bmatrix} \begin{bmatrix} u_1 \\ u_2 \\ p \end{bmatrix} = \begin{bmatrix} F_{1,\alpha} \\ F_{2,\alpha} \\ 0 \end{bmatrix} \quad (3.3)$$

where  $\vec{u} = (u_1, u_2)$ ,  $A_\alpha$ ,  $B_{1,\alpha}$ ,  $B_{2,\alpha}$  as well as  $M$  correspond to the usual velocity and pressure combinations in (2.23) and  $X^t$  it the transpose of  $X$ .

In the context of geometric refinements with irregular nodes we have to modify  $E_{K,\alpha}$  in order to account for these irregular nodes. HP90 is designed to enforce the appropriate constraints automatically on the local element stiffness matrix and load vector. This procedure [14] results in a modified local stiffness matrix  $\tilde{E}_{K,\alpha}$  that corresponds to the actual globally existing dof. This modified matrix  $\tilde{E}_{K,\alpha}$  can then be assembled to obtain the global stiffness matrix.

In the case of the G method the situation is somewhat more complicated due to the different approximation orders for the velocities and the pressure and additionally the pressure being discontinuous. Here we use the shape functions of order  $k$  on  $\hat{Q}$  to approximate the velocity components and the shape functions of order  $k-2$  to approximate the pressure. The dof for the velocity components are interpreted in the standard way but the pressure dof are now all interpreted as dof that belong to bubble shape functions, although the shape functions of order  $k-2$  contain vertex and side shape functions. It is obvious that the number of bubble shape functions of order  $k$  on  $\hat{Q}$  is exactly the same as the total number of shape functions of order  $k-2$ . This motivates to interpret  $\hat{Q}$  as a vector valued reference element with two components for the vertex and side dof and three components for the bubble dof and the shape functions being chosen as described above. The element computations for the G method are then again standard but we have to consider the unusual element definition. The local element stiffness matrix  $E_K$  is of a form similar to (3.3) with  $\alpha = 0$ . We further emphasize that we do not need the second derivatives of the shape functions to compute  $E_K$ . For an irregular mesh, i.e. irregular nodes being present, we again have to modify  $E_K$  to a local matrix  $\tilde{E}_K$  that corresponds to globally existing dof. But now we apply the constraints only to the velocity components because the pressure is discontinuous accross element boundaries. The element matrices  $\tilde{E}_K$  are then assembled in principle in the usual way but the non standard element definition requires a generalization of the assembling procedure to account for the presence of continuous and discontinuous field variables.

In both the G & GLS method we have to enforce Dirichlet boundary conditions that correspond to the boundary values of the exact solutions. The standard procedure very often used in practice is to interpolate the boundary data at equidistant points, but this procedure is known to be numerically instable for higher approximation orders. In connection with higher order methods interpolation at the Gauss Lobatto points is better suited (cf. [14]). We enforce the Dirichlet data for the G & GLS method in exactly the same way at the element level.

Although we apply Dirichlet boundary conditions to the velocity components, the global stiffness matrix is not invertible in both formulations, because the constant pressure mode is still not eliminated. To obtain invertibility of the global system we fix the pressure at one dof. Then the global system can be solved and we only have to postprocess the pressure so that the mean value is zero, i.e. so that the pressure is an element of  $L_0^2(\Omega)$ .

## 4 Numerical results for G & GLS $hp$ FEM

In the following we first describe the two model problems that we use. Both model problems have exact solutions and therefore allow for a numerical convergence study. These two exact solutions have significantly different characteristics, i.e. one solution is smooth and the other one has a corner singularity at the reentrant corner. These two model problems are well suited for a comparison of the G- and GLS-  $hp$ -FEM.

In our numerical results we present always the relative errors that we obtained with our  $hp$ -FE implementation. We show only the errors for the first velocity component (the results for the second one being completely similar) and the pressure. The velocity error is computed in the  $H^1$ -norm and the pressure error in the  $L^2$ -norm. In order to be consistent with the pressure being in  $L_0^2$ , we subtract the mean value from the exact pressure  $p$  and the numerical pressure  $p_N$ , i.e. we subtract terms of the form

$$\bar{p} = \frac{1}{|\Omega|} \int_{\Omega} p \, dx, \quad \bar{p}_N = \frac{1}{|\Omega|} \int_{\Omega} p_N \, dx, \quad (4.4)$$

and the relative error in the pressure is computed as

$$\frac{\|(p - \bar{p}) - (p_N - \bar{p}_N)\|_{L^2(\Omega)}}{\|p - \bar{p}\|_{L^2(\Omega)}}. \quad (4.5)$$

The relative  $H^1$ -error in the velocity components is computed in the standard way. We remark finally that the Gauss integration rule that we use to compute the errors is of significantly higher order than the integration rule in the element computations.

### 4.1 Model problems

In our model problems we consider the Stokes equation (2.1)-(2.3) with viscosity  $\nu = 1$  in the L-shaped domain  $\Omega$  shown in Figure 4. Such domains appear also in the backward facing step flow problem or in the so-called 4:1 contraction problem. On  $\Omega$  we use geometric meshes  $\mathcal{T}_{n,\sigma}$  with  $n + 1$  layers. Such a mesh (with irregular nodes) is shown for  $\sigma = 0.5$  in Figure 4.

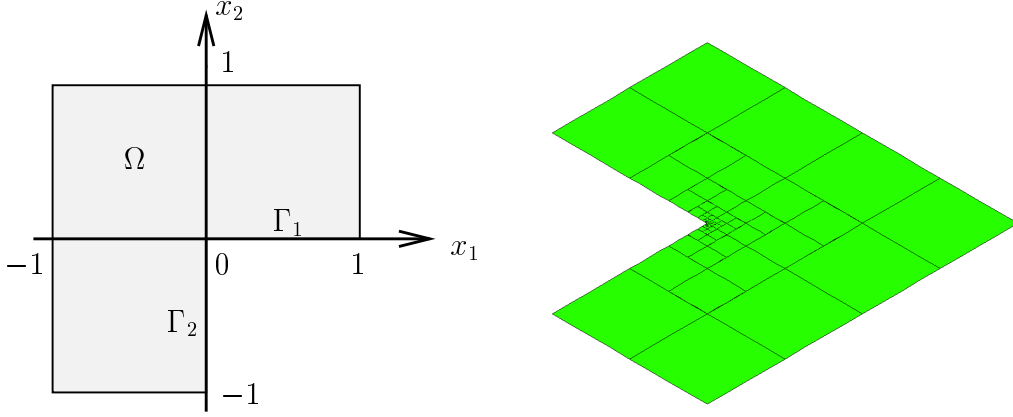


Figure 4: L-shaped domain  $\Omega$  and a geometric mesh on  $\Omega$ .

We use two exact solutions  $(\vec{u}_1, p_1)$  and  $(\vec{u}_2, p_2)$ , the first one exhibiting corner singularity phenomena at the reentrant corner 0, the second one being analytical in  $\bar{\Omega}$  (including the corners). In polar coordinates  $(r, \varphi)$  at the origin the first exact solution is given by (cf. [41, p. 113])

$$\vec{u}_1(r, \varphi) = r^\lambda \begin{pmatrix} (1 + \lambda) \sin(\varphi) \Psi(\varphi) + \cos(\varphi) \Psi'(\varphi) \\ \sin(\varphi) \Psi'(\varphi) - (1 + \lambda) \cos(\varphi) \Psi(\varphi) \end{pmatrix}, \quad (4.6)$$

$$p_1 = -r^{\lambda-1} [(1 + \lambda)^2 \Psi'(\varphi) + \Psi'''(\varphi)] / (1 - \lambda) \quad (4.7)$$

with

$$\begin{aligned} \Psi(\varphi) &= \sin((1 + \lambda)\varphi) \cos(\lambda\omega) / (1 + \lambda) - \cos((1 + \lambda)\varphi) \\ &\quad - \sin((1 - \lambda)\varphi) \cos(\lambda\omega) / (1 - \lambda) + \cos((1 - \lambda)\varphi), \\ \omega &= \frac{3\pi}{2}. \end{aligned}$$

The exponent  $\lambda$  is the smallest positive solution of

$$\sin(2\lambda\omega) + \lambda \sin(2\omega) = 0, \quad (4.8)$$

which is  $\lambda \approx 0.5444838205973307$ . This solution satisfies the homogeneous Stokes equation, i.e.  $-\Delta \vec{u}_1 + \nabla p_1 = 0$  in  $\Omega$ , and we have  $\vec{u}_1 = 0$  on the segments  $\Gamma_1, \Gamma_2$  shown in Figure 4. We emphasize that  $(\vec{u}_1, p_1)$  is analytical in  $\bar{\Omega} \setminus \{0\}$ , but  $\nabla \vec{u}_1$  and  $p_1$  are singular at the origin. Especially,  $\vec{u}_1 \notin H^2(\Omega)^2$  and  $p_1 \notin H^1(\Omega)$ .  $(\vec{u}_1, p_1)$  is of the form (2.28) and satisfies (2.27). This first solution reflects perfectly the typical (singular) behavior of solutions of the Stokes equations near reentrant corners.

The second exact solution we use is somehow artificial, since it is analytical in  $\bar{\Omega}$  (including the corners). In practice, one can not expect solutions to behave so nicely at reentrant corners. Nevertheless, smooth solutions arise for example in smooth domains and it is hence reasonable to validate the numerical performance for such exact solutions too. We take

$$\vec{u}_2(x, y) = \begin{pmatrix} -\exp(x)[y \cos(y) + \sin(y)] \\ \exp(x)y \sin(y) \end{pmatrix}, \quad (4.9)$$

$$p_2 = 2 \exp(x) \sin(y). \quad (4.10)$$

As above,  $-\Delta \vec{u}_2 + \nabla p_2 = 0$ .

## 4.2 Choice of $\alpha$ for the GLSFEM

The theoretical results in Section 2 guarantee stability of the GLSFEM as long as the parameter  $\alpha$  remains in a range  $0 < \alpha < \alpha_{max}$ .  $\alpha_{max}$  is independent of the element sizes  $h_K$  and the approximations orders  $k_K$  and is essentially given by the best constant  $C$  for which the inverse inequality

$$\|\nabla \pi\|_{L^2(\hat{K})} \leq C k^2 \|\pi\|_{L^2(\hat{K})} \quad (4.11)$$

holds on the reference element  $\hat{K}$  for all polynomials  $\pi \in \mathcal{S}^k(K)$  and all  $k \in \mathbb{N}$  (cf. [33]). In one dimension the best constant  $C$  in (4.11) is explicitly known and equal to  $3\sqrt{2}$  (if  $\hat{K} = (-1, 1)$ ). In two space dimensions this best constant seems not to be available, but we expect it to be of about the same order. In addition, one may ask whether this upper bound  $\alpha_{max}$  is just an artefact of the stability proof or whether it can really be observed in practice. On the other hand, we expect the GLSFEM to become unstable as  $\alpha$  approaches 0. In fact, for  $\alpha = 0$  the G- and GLS-discretization coincide and it is well known that the Galerkin method is unstable for velocity and pressure spaces of the same polynomial order.

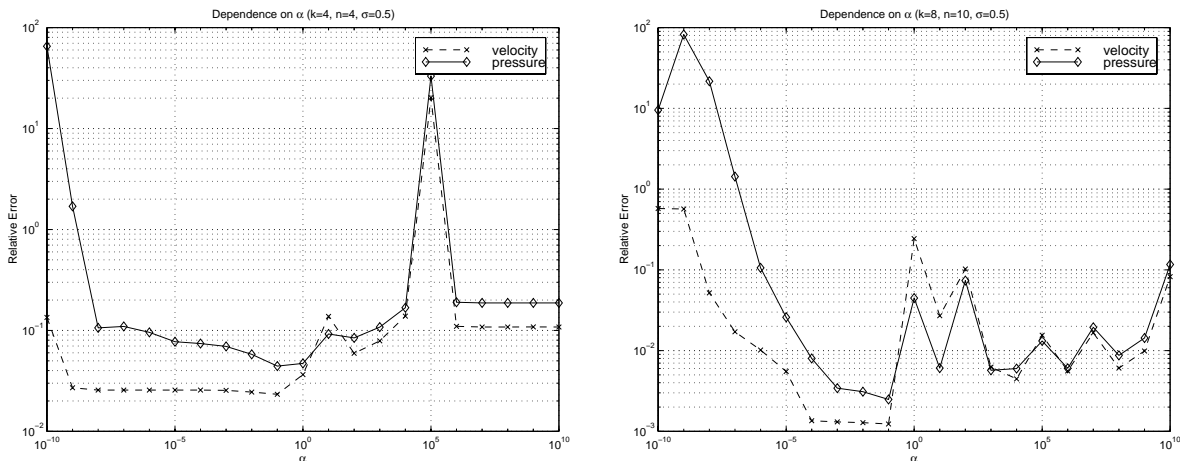


Figure 5: Dependence of the relative error on  $\alpha$ .

We addressed these questions numerically by varying  $\alpha$  in a large range. We considered two configurations for the model problem (4.6)-(4.7) in the L-shaped domain, the first one being  $k = 4$ ,  $n = 4$  and  $\sigma = 0.5$ , the second one  $k = 8$ ,  $n = 10$  and  $\sigma = 0.5$ , where  $k$  is the polynomial degree and  $n$ ,  $\sigma$  determine the geometric mesh  $\mathcal{T}_{n,\sigma}$  with  $n + 1$  layers and grading factor  $\sigma$ . In Figure 5 the relative errors of the first velocity component and the pressure are plotted for these two configurations against  $\alpha$  ranging from  $10^{-10}$  to  $10^{10}$ . Very soon the error curves become oscillatory for increasing  $\alpha$ . The “existence” of an upper bound  $\alpha_{max}$  can not be answered affirmatively with absolute certainty. Anyway, the performance of the GLSFEM is rather poor in the range  $\alpha \geq 10^0$ . But the deterioration of the GLS-scheme as  $\alpha$  approaches zero can indeed be observed:

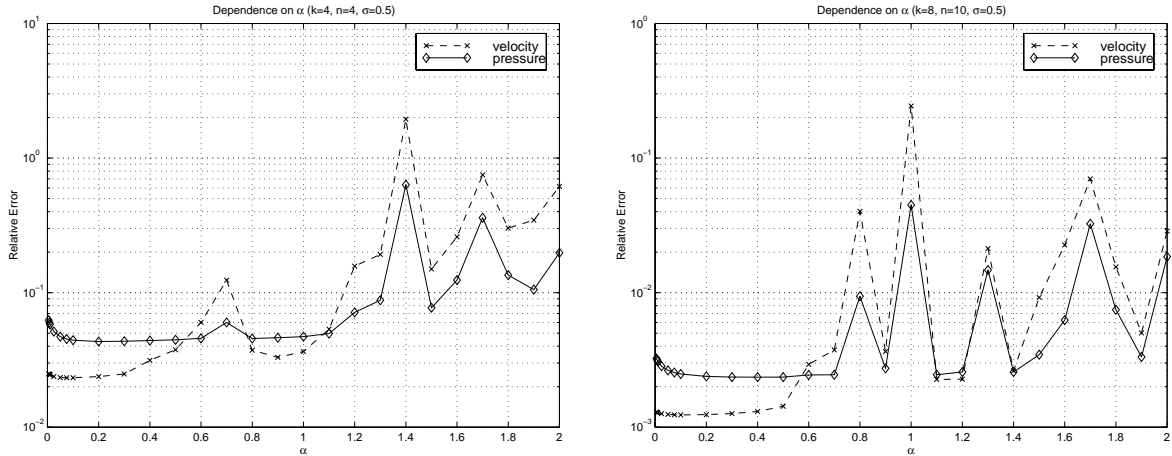


Figure 6: Dependence of the relative error on  $\alpha$  .

The errors begin to grow and finally to explode for  $\alpha \leq 10^{-5}$ . In this range the velocities are still more or less accurate but the obtained pressures become strongly oscillatory. This phenomena already mentioned in [21] is reasonable since the pressure terms are in fact the terms that are stabilized. It can be seen that the best results are obtained for  $\alpha \in (10^{-5}, 10^0)$ . This range is depicted separately in Figure 6 and therein the scheme seems to be more or less robust in the parameter  $\alpha$ . Therefore, in all our numerical results that we present in the following we use  $\alpha = 0.1$ .

### 4.3 Numerical experiments for the smooth solution

In Figure 7 we present convergence rates for the  $h$ - and  $p$ -version G & GLSFEM that we obtained by approximating the smooth solution (4.9)-(4.10) to the Stokes problem. In the  $h$ -version we use uniform meshes and expect convergence rates as in (2.30) and (2.31). The approximation order for the velocity is chosen to be cubic and this implies a linear approximation of the pressure in the G method. We start with 3 elements in the L-shaped domain and uniformly  $h$ -refine the mesh. Note that the meshwidth  $h$  is given by  $CN^{\frac{1}{2}}$ , where  $N$  is the number of dof. It is evident from Figure 7 that the  $h$ -version yields a convergence rate of 2 for the G method, which is in agreement to (2.31). For the GLS method the  $h$ -version convergence rate is 3, which is optimal, compare (2.30). Since the exact solution (4.9)-(4.10) is analytic in  $\bar{\Omega}$ , we expect exponential convergence of the  $p$ -version. We start again with a 3 element mesh and increase the polynomial approximation order from 3 to 8 for the velocity. Here, we have  $p \approx N^{\frac{1}{2}}$ . The convergence rates displayed in Figure 7 indicate the exponential convergence of the G & GLS FEM for this smooth solution.

### 4.4 Numerical experiments for the singular solution

In this section we present numerical results for the first model problem (4.6)-(4.7). We recall that the solution has a singularity at the reentrant corner. Therefore, it is

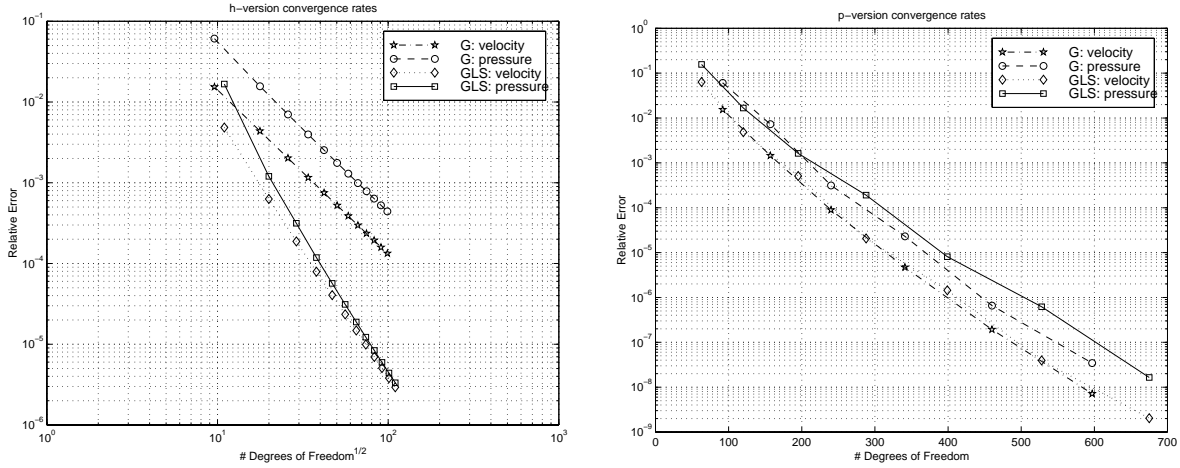


Figure 7:  $h$ - and  $p$ -version G & GLS FEM convergence rates.

necessary to perform mesh refinements towards the singularity in order to capture the singular behavior of the exact solution. In Figures 8 to 11 we present convergence rates that correspond to meshes of affine elements that have been refined geometrically towards the reentrant corner with a grading factor of  $\sigma = 0.5$ . An example of such a mesh is displayed in Figure 4. This mesh contains  $l = 8$  layers of elements, which have been generated by successively refining 3 initial elements. The irregular nodes in this mesh are constrained automatically by HP90.

In Figures 8 and 9 we show the performance of the  $p$ -version FEM by fixing a grid with  $l$  layers, and increasing the polynomial approximation order  $k$  from 3 to 8. As to be expected with the  $p$ -version, the graphs indicate algebraic rates of convergence which in fact are very close to the a-priori bound of  $k^{0.5-2\lambda} \approx N^{0.25-\lambda}$ , where  $\lambda$  is the constant in (4.8). This a-priori bound is optimal in view of [4] and the fact that the inf-sup constant (2.18) is  $Ck^{-0.5}$  in the G method [8, 39]. In Figure 9 the same plot is depicted

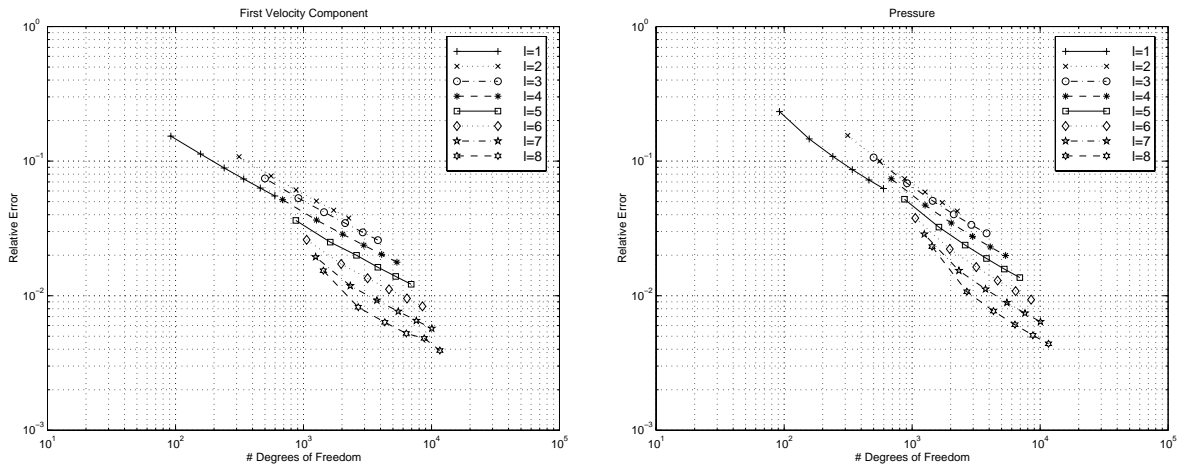


Figure 8:  $p$ -version GFEM convergence rates for geometric meshes with hanging nodes.

for the GLSFEM and shows a convergence similar to the GFEM. This indicates that the dependence of the inf-sup constant on the approximation order in (2.26) is probably suboptimal. We expect the  $p$ -version of the GLSFEM to be comparable to the GFEM, however, the corresponding theoretical results have to be established.

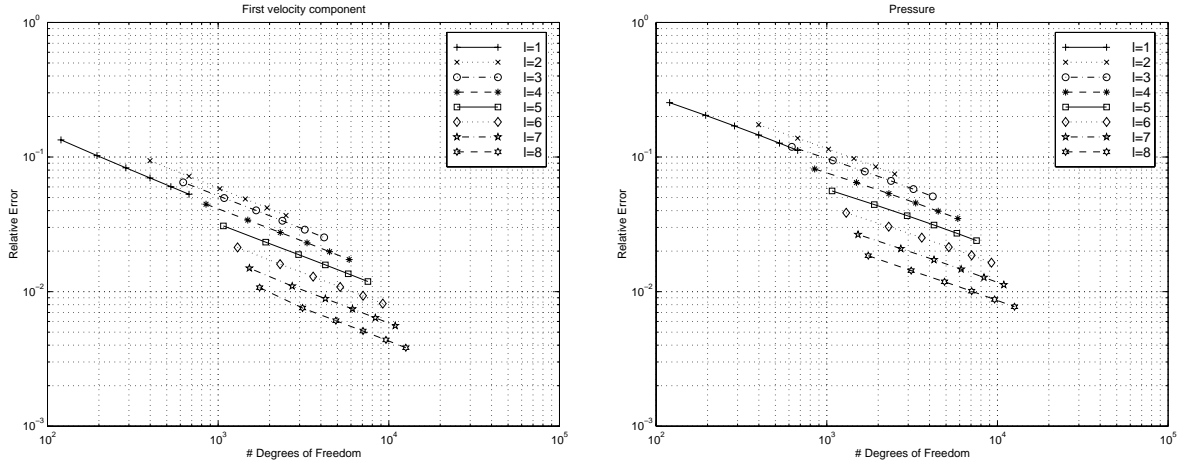


Figure 9:  $p$ -version GLSFEM conv. rates for geometric meshes with hanging nodes.

For the  $hp$ -version we show the convergence rates in Figures 10 and 11. Here we do not only vary the polynomial degree but also the grid, i.e. the number of layers in the mesh. We do this with respect to the parameter  $\mu$  (cf. Remark 2.6), where

$$l = \mu \cdot k. \quad (4.12)$$

Again, here  $l$  is the number of layers and  $k$  the polynomial degree. If  $\mu \cdot k$  is not an integer, then we round it to the nearest integer. The  $hp$  convergence rates for various parameters  $\mu$  indicate the exponential convergence of the  $hp$ -version, as expected and predicted by Theorem 2.4.

The affine geometric meshes with hanging nodes are obtained by bisecting elements in the middle, which results in a mesh grading factor of  $\sigma = 0.5$ . With this  $\sigma$  we obtain reliable results, but the optimal grading factor is  $\sigma \approx 0.15$  in one dimension [2]. Although the optimal  $\sigma$  is not explicitly known for two dimensions, we expect it to be of approximately the same order. To study the dependence on  $\sigma$ , we use geometric meshes with variable order elements that have bilinear element mappings. An example mesh with geometric refinement toward the reentrant corner with  $\sigma = 0.3$  and 8 layers of elements is shown in Figure 12. We emphasize that there are really 8 layers of elements because the elements in the layers at the reentrant corner are so small that they are not visible in Figure 12.

We demonstrate the dependence of the GFEM on the geometric mesh grading in Figure 13. It can be seen that the  $hp$ -version GFEM is converging exponentially for all values of  $\sigma$  on these geometric meshes. Further, the performance is best for  $\sigma = 0.15$  and  $\sigma = 0.2$ , which are very close to the optimal  $\sigma$  in one dimension. In particular, for  $\sigma = 0.5$  the error is about one order of magnitude larger than for the optimal grading factor. The best result with  $\sigma = 0.5$  is obtained with  $N \approx 5000$  while for  $\sigma = 0.15$

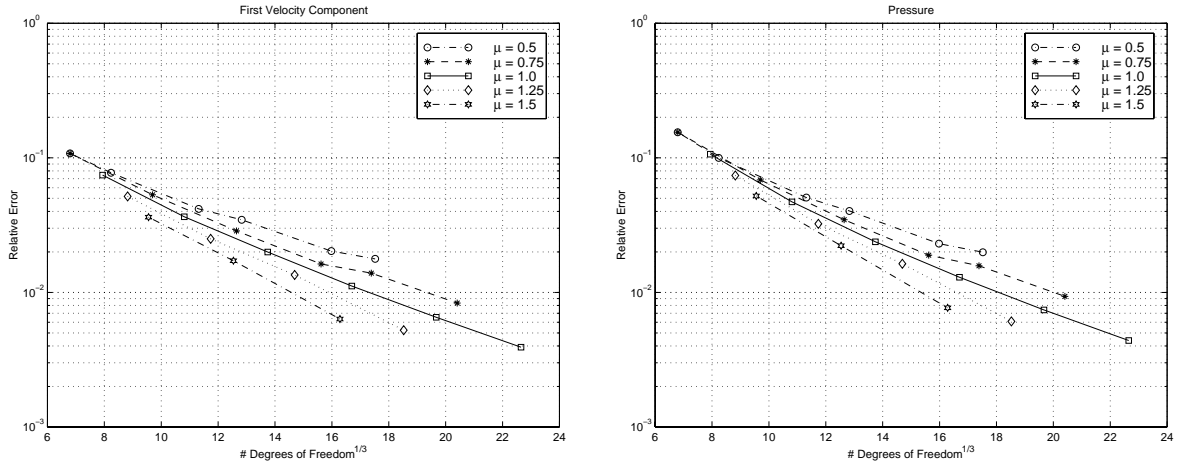


Figure 10:  $hp$ -version GFEM conv. rates for geometric meshes with hanging nodes.

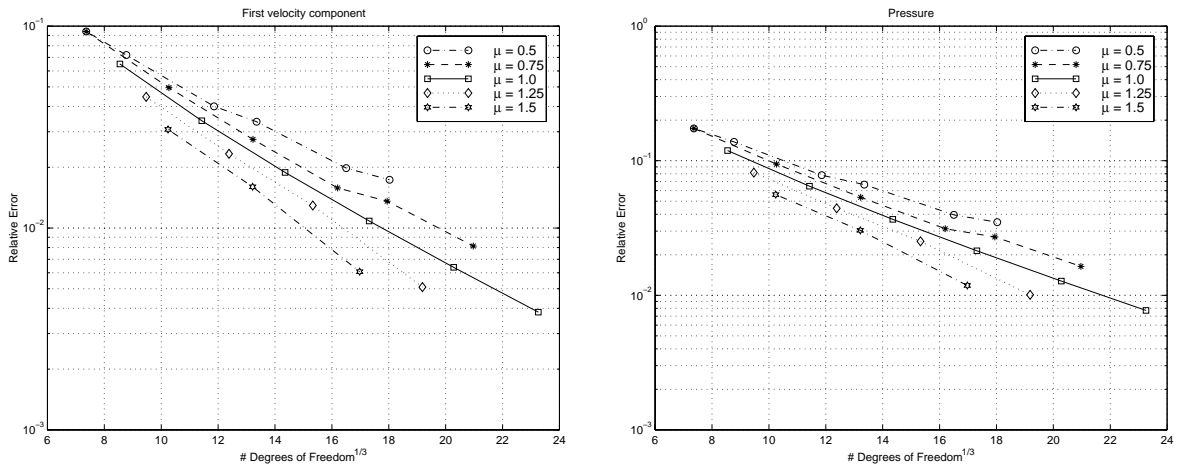


Figure 11:  $hp$ -version GLSFEM conv. rates for geometric meshes with hanging nodes.

the same accuracy is already obtained with 1500 dof. This supports the importance of refining towards the singularity with the grading factor 0.15.

## 5 Conclusions

In this work we have studied stable and stabilized  $hp$ -FE approximations for the Stokes problem. For both the stable GFEM and the stabilized GLSFEM we presented theoretical results of exponential convergence, which rely on geometric mesh refinement. The geometric meshes as well as the corresponding  $hp$ -FE spaces are described in this work. Details of the non standard  $hp$  implementation are given for both methods.

The numerical results obtained on an  $L$ -shaped domain are consistent with the theoretical estimates and demonstrate clearly the exponential convergence of both methods.

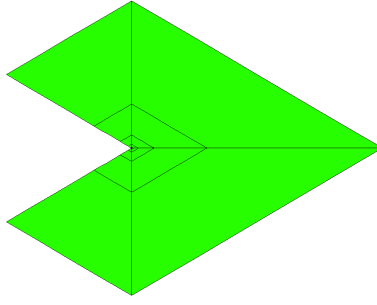


Figure 12: Geometric mesh with 8 layers of elements.

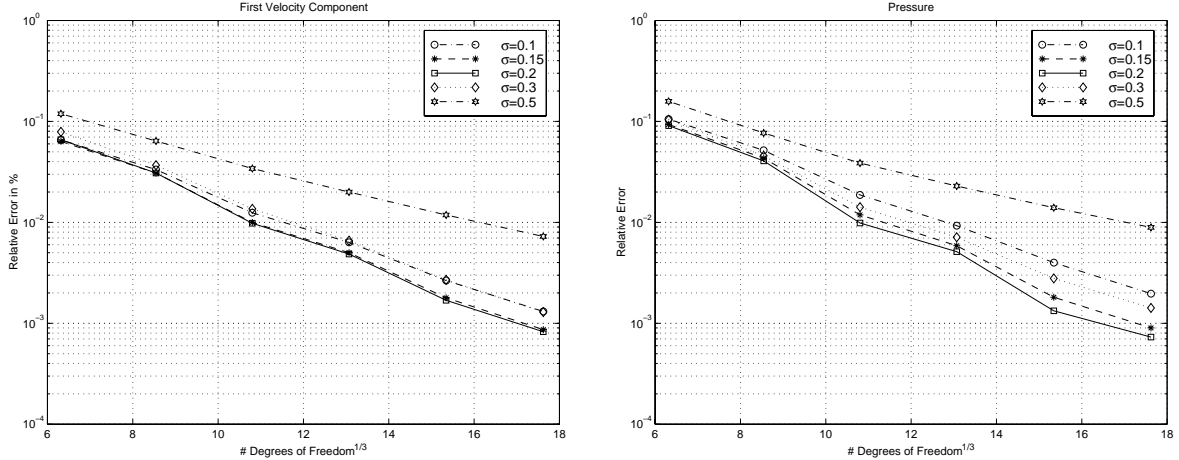


Figure 13:  $hp$ -version GFEM convergence rates for geometric meshes with  $\mu = 1$  and varying  $\sigma$ .

For the GLSFEM the stabilization factor  $\alpha$  can be chosen independently of the element sizes and the approximation orders and, in a certain range, this method gives robust results. Further, the question of the optimal grading factor is addressed and our numerical experiments confirm the optimal one-dimensional mesh grading results.

The general code HP90 [14] was used for the computations. This implementation allows for a variable polynomial approximation order of up to eight and geometric meshes with possibly irregular nodes. From the implementational point of view we remark that the GLS method provides the convenient setting of equal order continuous FE spaces for all field variables, whereas this is not the case in the mixed Galerkin approach. On the other hand, it is necessary to compute the second derivatives of the shape functions in the GLS method, which is not necessary in the G method. In our G & GLS implementation there was no significant conceptual difference in implementing either one of them and also in the  $hp$  context stabilized methods represent a competitive alternative to stable elements.

## References

- [1] M. Ainsworth and J. T. Oden. A posteriori error estimators for the Stokes and Oseen equations. *SIAM J. Numer. Anal.* 34 (No. 1) (1997), 228-245.
- [2] I. Babuška and W. Gui. The  $p$  and  $hp$  versions of the finite element method in one dimension. Part I: the error analysis of the  $p$  version. Part II: the error analysis of the  $hp$  version. *Numer. Math.* 49, 577-612 and 613-657.
- [3] I. Babuška and B.Q. Guo. Regularity of the solution of elliptic problems with piecewise analytic data I,II. *SIAM J. Math. Anal.* 19 (1988), 172-203, and 20 (1989), 763-781.
- [4] I. Babuška and M. Suri. Optimal convergence rate of the  $p$ -version of the Finite Element Method. *SIAM J. Numer. Anal.* 24 (1987), 750-776.
- [5] I. Babuška and M. Suri. The  $p$ - and  $hp$ -versions of the finite element method: an overview. *Computer Methods in Applied Mechanics and Engineering* 80 (1990), 5-26.
- [6] R. Becker. An adaptive FEM for the incompressible Navier-Stokes Equations on time dependent domains. Preprint 95-44, IWR, Univ. Heidelberg, 1995.
- [7] R. Becker and R. Rannacher. Finite element solution of the incompressible Navier-Stokes equations on anisotropic refined meshes. Proc. of the 10th GAMM Seminar, *Notes on Num. Fluid Dyn.*, Vieweg Publ. Braunschweig, Germany, 1995.
- [8] C. Bernardi and Y. Maday. *Approximations spectrales de problèmes aux limites elliptiques*. Springer Verlag, Paris-New York, 1992.
- [9] C. Bernardi and Y. Maday. Preprint.
- [10] E. Boillat and R. Stenberg. An  $hp$  Error Analysis of some Galerkin Least Squares Methods for the Elasticity Equations. Research Report 21-94, Helsinki University of Technology, 1994.
- [11] F. Brezzi and J. Douglas, Jr. Stabilized mixed methods for the Stokes problem. *Numer. Mathematik* 53 (1988), 225-236.
- [12] F. Brezzi and M. Fortin. *Mixed and hybrid Finite Element Methods*. Springer Series in Comp. Mathematics 15, Springer Verlag, New York, 1991.
- [13] C. Canuto, M. Y. Hussaini, A. Quarteroni and T. A. Zang. *Spectral Methods in Fluid Dynamics*. Springer Verlag, 1988.
- [14] L. Demkowicz, K. Gerdes, C. Schwab, A. Bajer and T. Walsh. HP90: A general & flexible Fortran 90  $hp$ -FE code. SAM Report 97-17, ETH Zürich, 1997.
- [15] J. Douglas, Jr. and J. Wang. An absolutely stabilized finite element method for the Stokes problem. *Math. Comp.* 52 (1989), 495-508.

- [16] L.P. Franca, T.J.R. Hughes and R. Stenberg. Stabilized Finite Element Methods. *Incompressible Computational Fluid Dynamics: Trends and Advances*, editors M.D. Gunzburger and R.A. Nicolaides, Cambridge University Press, 1993.
- [17] L.P. Franca and R. Stenberg. Error analysis of some Galerkin-least-squares methods for the elasticity equations. *SIAM J. Num. Anal.* 28 (No. 6) (1991), 1680-1697.
- [18] P. Gervasio and F. Saleri. Stabilized Spectral Element Approximation for the Navier-Stokes Equations. *Numerical Methods for Partial Differential Equations* 14 No.1 (1998), 115-141.
- [19] V. Girault and P.-A. Raviart. *Finite Element Methods for Navier-Stokes Equations*. Springer-Verlag, 1986.
- [20] B.Q. Guo and I. Babuška. The  $hp$ -version of the finite element method I: The basic approximation results; and part II: General results and applications. *Comp. Mech.* 1 (1986), 21-41 and 203-226.
- [21] T.J.R. Hughes, L.P. Franca and M. Balestra. A new finite element formulation for computational fluid dynamics: V. Circumventing the Babuška-Brezzi condition: A stable Petrov-Galerkin formulation of the Stokes problem accomodating equal-order interpolations. *Computer Methods in Applied Mechanics and Engineering* 59 (1986), 85-99.
- [22] I. Lomtev, C. B. Quillen and G. E. Karniadakis. Spectral/ $hp$  Methods for Viscous Compressible Flows on Unstructured Meshes. Report 96-12, Center for Fluid Mechanics, Brown University.
- [23] Oden, Demkowicz, Rachowicz and O. Hardy. Toward a Universal  $h - p$  Adaptive Finite Element Strategy. Part 1: Constrained Approximation and Data Structure. *Computer Methods in Applied Mechanics and Engineering* 77 (1989), 79-112.
- [24] J. T. Oden and O. Jacquotte. Stability of some mixed finite element methods for Stokesian flows. *Computer Methods in Applied Mechanics and Engineering* 43 (1984), 231-247.
- [25] J. T. Oden and L. Demkowicz.  $hp$  adaptive finite element methods in computational fluid dynamics. *Computer Methods in Applied Mechanics and Engineering* 89 (1991), 11-40.
- [26] J. T. Oden. Error Estimation and Control in Computational Fluid Dynamics. *The Mathematics of Finite Elements and Applications*, MAFELAP VIII; edited by J. Whiteman, John Wiley & Sons, Strasbourg, 1994, 137-149.
- [27] J. T. Oden, T. Liszka and W. Wu. An h-p Adaptive Finite Element Method for Incompressible Viscous Flows. *The Mathematics of Finite Elements and Applications VII*, J. Whiteman (ed.), Academic Press Limited, 1991, 13-54.
- [28] J. T. Oden, W. Wu and M. Ainsworth. An A Posteriori Error Estimate for Finite Element Approximations of the Navier-Stokes Equations. *Computer Methods in Applied Mechanics and Engineering* 111 (1994), 185-202.

- [29] A. Patra and J. T. Oden. Problem Decomposition For Adaptive  $hp$  Finite Element Methods. *Computer Systems in Engineering* 6 (1995), 97-109.
- [30] A. Patra, A. Parallel  $hp$  adaptive finite element analysis for viscous incompressible flow problems. Ph.D. Dissertation. The University of Texas at Austin, 1996.
- [31] W. Rachowitz. An anisotropic  $h$ -type mesh-refinement strategy. *Computer Methods in Applied Mechanics and Engineering* 109 (1993), 169-181.
- [32] S. J. Sherwin and G. E. Karniadakis. A triangular spectral element method; applications to the incompressible Navier-Stokes equations. *Computer Methods in Applied Mechanics and Engineering* 123 (1995), 189-229.
- [33] D. Schötzau, K. Gerdes and C. Schwab. Galerkin Least Squares  $hp$ -FEM for the Stokes problem. *Comptes Rendus de l'Académie des Sciences Paris*, t. 326 (1998), Série I, 249-254.
- [34] D. Schötzau, C. Schwab and R. Stenberg. Mixed  $hp$ -FEM on anisotropic meshes II: Hanging nodes and tensor products of boundary layer meshes. SAM Report 97-14, ETH Zürich, 1997.
- [35] C. Schwab and M. Suri. The  $p$  and  $hp$  versions of the finite element method for problems with boundary layers. *Math. Comp.* 65 (1996), 1403-1429.
- [36] C. Schwab and M. Suri. Mixed  $hp$ -FEM for incompressible fluid flow. Mixed  $hp$ -Finite Element Methods for Stokes and Non-Newtonian Flow. SAM Report 97-19, ETH Zürich, 1997, in press in *Computer Methods in Applied Mechanics and Engineering*.
- [37] C. Schwab, M. Suri and C. A. Xenophontos. The  $hp$ -version of the FEM for problems in Mechanics with boundary layers. SAM Report 96-20, ETH Zürich, 1996, in press in *Computer Methods in Applied Mechanics and Engineering*.
- [38] R. Stenberg. Error Analysis of some Finite Element Methods for the Stokes problem. *Math. Comp.* 54 (1990), 495-508.
- [39] R. Stenberg and M. Suri. Mixed  $hp$  Finite Element Methods for problems in elasticity and Stokes flow. *Num. Math.* 72 (1996), 367-389.
- [40] B. Szabó and I. Babuška. *Finite Element Analysis*. Wiley, 1991.
- [41] R. Verfürth. *A review of a posteriori error estimation and adaptive mesh-refinement techniques*. Wiley-Teubner, Chichester-Stuttgart, 1996.
- [42] W. Wu. H-P adaptive methods for incompressible viscous flow problems. Ph.D. Dissertation. The University of Texas at Austin, 1993.

DRAFT